Determination of Scaling Zone and Scaling Type in Slotted Liner Based on the Fluid Flow Pattern in the Geothermal Well "X"

Akhmad Sofyan*, **‡, Syafira Wiharti**, János Szanyi****, Bambang Yudho Suranta**, Rita Njeru***

*Department of Mineralogy, Geochemistry and Petrology, Faculty of Earth Science, University of Szeged, 13 Dugonics Square Szeged 6722, Hungary

**Politeknik energi dan mineral Akamigas, Jalan Gajahmada No.38 Cepu, 58315, Indonesia

***Department of Mineralogy, Geochemistry and Petrology, Faculty of Earth Science, University of Szeged, 13 Dugonics Square Szeged 6722, Hungary

****Department of Mineralogy, Geochemistry and Petrology, Faculty of Earth Science, University of Szeged, 13 Dugonics Square Szeged 6722, Hungary

(akhmad.sofyan@geo.u-szeged.hu, syafirawiharti@gmail.com, szanyi@iif.u-szeged.hu, yudho_bys@yahoo.com, mwenderita@gmail.com)

‡Corresponding Author; Akhmad Sofyan, Department of Mineralogy, Geochemistry and Petrology, Faculty of Earth Science, University of Szeged, 13 Dugonics Square Szeged 6720, Hungary, Tel: +36 20 3922897,

Fax: +36 62 426479, akhmad.sofyan@geo.u-szeged.hu

Received: 04.11.2022 Accepted:.12.2022

Abstract- A geothermal well can experience a decrease in the production of fluid (steam) due to the presence of scaling. The scaling usually is formed in the slotted liner hole. The purposes of this study were to determine the fluid flow pattern, the zone of scaling accumulation, and the scaling type in the well "X". This can be a reference to determine the next step to prevent and clean scaling problems in the wellbore. In determining the fluid flow pattern, the manual calculation using the Hewitt-Robert method and the simulation calculation using WellSim software were conducted. In determining the zone of scaling accumulation, the pressure, temperature, and spinner (PTS) survey data were utilized. In determining the scaling type, the geochemical analysis data were utilized. The results showed that the fluid flow pattern was annular flow based on the Hewitt-Robert method and mist flow based on WellSim software. There is no flow pattern type of mist in the grouping of flow patterns based on Hewitt-Robert. Because the characteristics of mist flow and annular flow are almost the same, the annular flow pattern can be considered similar to mist flow. Furthermore, the results were validated with PTS survey data so that the flashing zone was known at a depth of 1458.27 m from a total depth of 1700 m. Based on the geochemical analysis, it was known that the scaling type in the well "X" is of the calcite type.

Keywords Flow Pattern, Geothermal, Production, Scaling, Slotted Liner.

1. Introduction

Geothermal energy is different from other natural energies such as oil, natural gas, minerals, and coal because it cannot be transported and can only be used for the development of production [1]. This energy can only be produced at a given time, needs to be reserved, and is not available everywhere [2]. However, The Geothermal energy is a replenished source and can be utilized all year round [3]. Because of that, the potential of geothermal energies is necessary to be investigated and discovered [4]. In addition, The geothermal energy establish an opportunity for fulfil the needs of future generations [5]. In 2021, the total geothermal potential in Indonesia reaches 23,765.5 Megawatt equivalent (Mwe) or around 40% of the total geothermal potential in the world. Currently, geothermal potential in Indonesia has only

been utilized at 4.5%, meaning that there is still around 95.5% of Indonesian geothermal potential that has not been utilized. Therefore, the government has set a target to increase geothermal consumption to 23% by 2025 [6].

Along with the increasing energy consumption and demand due to changes in population growth and lifestyle [7], the production of geothermal energy as alternative energy needs to be increased to full fill the national energy target in the year 2025. Several steps are carried out for the development of geothermal energy, namely the preliminary 3G survey (geology, geochemistry, geophysics), exploration 3G survey, exploration drilling, project review and planning, field development, power plant construction, commissioning, and operation [8].

In utilizing geothermal energy, geothermal fluid that has been released to the surface of the earth contains heat energy which will be used to generate electrical energy. The fluid originates from the geothermal reservoir layer which is formed as a result of heat transfer from a heat source to its surroundings which occurs by conduction and convection [9].

Each reservoir layer in the earth contains a variety of different characteristics such as fluid and rock content and rock hardness levels, so it is very important to research to find the right method to solve problems at each reservoir location. Some of the challenges faced when geothermal energy is produced from deep wells are the most common problems have been related to the chemistry of the geothermal fluids which sometimes contain quite considerable concentrations of minerals and gases, which can cause scaling and corrosion in wells and surface installations which the geothermal fluids flow through [10].

Formation of scaling in geothermal wells is one of the main factors that can lead to a decrease in the quality and quantity of energy production because it can cause damage to pipes and reduce production speed. Scaling is deposits or solids in a reservoir or along a flow pipe of geothermal energy production which is formed due to changes in pressure, temperature, and pH in a liquid system. The type of scaling is affected by the chemical composition of the liquid in the system [11]. The accumulation zone of scaling and the cause of scaling can be determined by analyzing the flow pattern and characteristics of the fluid (steam) in the geothermal wells.

Scaling usually occurs in the casing series. In a geothermal well ”X”, it is known that there is a blockage by scaling in the slotted liner hole which can reduce the amount of geothermal energy production. Therefore, the cause of the decline in geothermal energy production from the well “X” must be analyzed by determining the accumulation zone of scaling and the cause of scaling by determining the fluid flow pattern found in the well “X”[12]. This can be a reference to determine the next step to prevent and clean scaling problems in the wellbore.

Research on determining fluid flow patterns was carried out in Banjarmasin in 2015 to examine the effect of salt concentration on the flow characteristics of two-phase fluid (gas-liquid fluid) using Hewitt-Robert calculation method for flow pattern mapping. The results showed that the flow pattern before flooding was annular and it during flooding was churn [13]. The other related research conducted by Flores Amenta in 2015 was about determining the flow pattern using WellSim software to establish the thermodynamic state of the fluid at any given depth to investigate the cause of decline production in the wellbore [14]. Furthermore, research conducted by Tolivia (1972) reported that by analyzing the flow pattern, the formation of scaling can be predicted in the well “Y”. There are two types of scaling in the well, namely silica scaling and calcite scaling [15]. The silica scaling dissolves in the high-temperature well, evaporates from the liquid phase, and then settles on the casing wall of the well. At the same time, the calcite scaling, which does not dissolve in liquid, will lose carbon dioxide (CO_2) and becomes calcium carbonate ($CaCO_3$). This loss of carbon dioxide is caused by a decrease in pressure because the solubility of the gas in the liquid is proportional to the pressure (Henry's Law). These two phenomena of scaling occur along the wellbore and in the annular flow zone where boiling of the fluid on the casing wall can increase the accumulation of the two scales [15]. However, the research conducted by Widodo et al. (2015) did not use data on actual conditions in the field [13]. Furthermore, research conducted by Widodo et al. (2015) and Tolivia (1972) did not perform simulations using the Wellsim software. Meanwhile, the research conducted by Flores Amenta can determine the flow pattern along the section of the well to differentiate separated (nonhomogenous) flow from the homogenous flow but it was not related to determining the type of fluid flow pattern that has the potential to cause scaling[14]. In year 2020, Zolfagharroshan and Khamehchi has conducted a research to predicts scale precipitation and deposition during drilling in addition to modeling production conditions using two-phase fluid flow equations with HOLA software. However, this research not determining the flow pattern that can cause the scaling in the wellbore [15] . Therefore, current research is important to do to cover the shortcomings in the previous studies.

This research used Hewitt-Robert calculation method to find out the fluid flow patterns that occur in the wellbore (the well “X”) and was also validated using the Wellsim software. Wellsim is a geothermal wellbore simulator that can analyze the types of flow patterns at each wellbore depth. In addition to knowing the flashing zone that occurred in the wellbore, this study used the Pressure, Temperature, and Spinner (PTS) survey data obtained from the field. Furthermore, the object used in this research was the fluid from a geothermal reservoir (the well “X”). Meanwhile, the previous research used salt water as a research object and was carried out on the pipeline surface with the Dukler equation method [15]. Therefore, this research is new and has not been conducted by other researchers yet.

The objectives of this study were (1) to determine the fluid flow pattern formed from the geothermal well “X”, (2) to determine the accumulation zone of scaling in the well based on PTS survey data, (3) to determine the type of fluid flow pattern that has the potential to cause scaling, (4) to determine the type of scaling formed in the well.

2. Methods

The flow chart of this research is shown in detail in Figure 1.

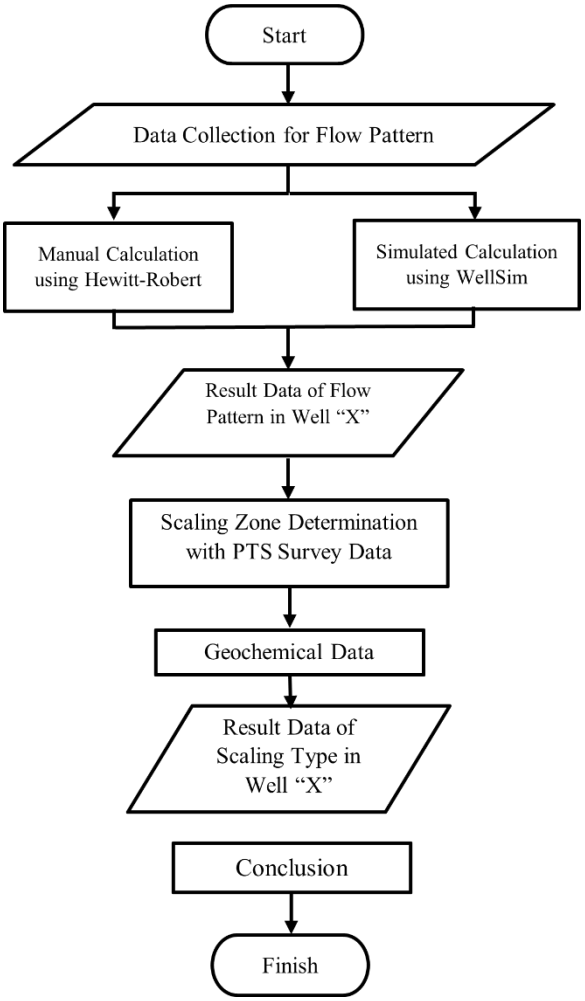

Fig. 1. Flowchart of the research.

The data used in this research were real data collected from the real geothermal field from 3rd February 2022 to 3rd May 2022, as following: geochemical data, PTS data, well's head pressure data, well's production data, flow rate data, well's profile data, and casing summary data.

The data analysis process as shown in the Figure 1 was carried out after all the necessary data were collected. Then, the flow pattern was determined based on the coordinates of the calculation which was calculated manually using the Hewitt-Robert method. To validate the results obtained from the Hewitt-Robert method, the WellSim software was used to simulate the flow pattern, so that the results from the manual calculation and simulated calculation can be compared to determine the final type of fluid flow pattern in the well "X".

Furthermore, determining the depth of the flashing zone was carried out using the PTS survey data so the accumulation zone of scaling in the slotted liner in the well "X". By knowing the flashing zone in the well, scaling at a certain depth can be estimated because the fluid in the well "X" experiences change in pressure, temperature and pH.

After knowing the flashing zone, geochemical analysis was carried out to determine the type of scaling in the well "X". This was done to prove that there was scaling in the well "X" after knowing the flashing zone and flow pattern.

2.1. Manual Calculation using Hewitt-Robert Method

Determination of the fluid flow pattern in the well "X" was manually carried out using the Hewitt-Robert method.

This process requires some data, namely pressure, depth, flow rate, enthalpy, dryness pipe, and diameter. Then it is calculated by a formula based on the Hewitt-Robert method to get the cross-sectional area of the well "X". It is applied to get the coordinates of the x and y flow patterns. From these coordinates will determine the flow pattern in well "X".

2.2. Simulation using WellSim Software

In the calculation process using WellSim, some data are needed, namely well deviation, casing configuration, geometry configuration, and feed zone. Then it starts the discharge simulation calculation to find the flow pattern results in well "X".

2.3. Geochemical Analysis

Water and gas from the geothermal well were analyzed and the samples were obtained from the downhole tube sampler with Klyen methode. The cations and anions were analyzed using ion chromatography, ICP-OES, alkalimetric titration, and spectrophotometry, while isotopes were measured using a Liquid Water Isotope Analyzer [16].

After the tube sampler returned to the surface and was cooled down, the gas and aqueous samples were separated into different containers. The gas sample was induced and stored in another prevacuum stainless tube sampler, and the aqueous sample was separated into three distinct bottles, one for on-site measurement, one for anion analysis and one for cation analysis. The aqueous sample for cation analysis was acidified in the field with ultra-pure nitric acid to pH < 2. The temperature, pH value, redox potentials (Eh) and electrical conductivity (EC) of the aqueous sample were immediately measured in the field with the electrochemistry meter. Alkalinity was also analysed in situ by titration with hydrochloric acid. The gas and remaining aqueous samples were sent to laboratories for chemical analysis. The aqueous samples were analysed by ion chromatography for anion analysis and by induced coupled plasma-mass spectroscopy for cation analysis [17]. The collected gas sample was then taken to the laboratory for analysis. Analysis of gas samples was carried out by two methods i.e. gas chromatography method for inactive gases (H_2, Ar, N_2, and CH_4) and GC titration method for reactive gases (CO_2, NH_3, and H_2S) [13].

3. Results and Discussions

The well "X" is a steam-dominated well that has a depth of up to 1700 meters with an energy production capacity of 12 MW and a dryness of 98% located in Patuha. The well "X" has production casings of 20" and 13 3/8" and perforated liners of 10 3/4" and 7", which can be seen in Figure 2.

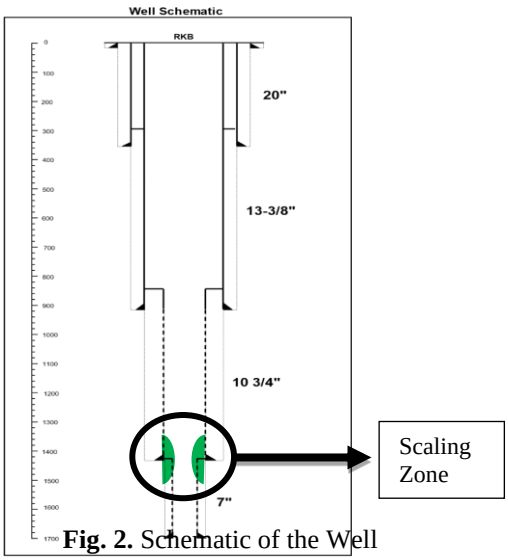

Fig. 2. Schematic of the Well

3.2. Determination of Flow Pattern Using the Hewitt-Robert Method

Determination of the vertical fluid flow pattern in the well "X" was conducted using Hewitt-Robert flow pattern mapping because the steam and hot water fluid flow upward (vertical up flow) with a pressure range of atmospheric pressure up to 1000 psi. The steps to determine the vertical flow pattern are as follows:

3.2.1. Determination of the Cross-Sectional Area of the Flow Pipe in the Well "X"

The cross-sectional area of the flow pipe in this analysis was the cross-sectional area of the entire casing in the well "X" from the surface to a depth of 1700 meters. Along the depth of the well, there were 20" and 13 3/8" production casings, then 10 3/4" and 7" perforated liners.

For example, the cross-sectional area of the flow pipe of the casing of 13 3/8" with an inner diameter of 12.415 in (1 in = 0.0254 m) can be calculated through the formulation below:

$$Ap = \pi \frac{di^2}{4} \quad (1)$$

$$Ap = 3.14 \frac{(12.415 \times 0.0254)^2}{4}$$

$$Ap = 0.078\, m^2$$

Where:

Ap, the cross-sectional area (m^2); π, constants; *di*, diameter inside of the casing (m)

Based on the Figure 4, the calculation of the cross-sectional area of the flow pipe in the well "X" used the top casing first, namely the production casing of 13 3/8" with an inner diameter of 12.415 in, because the production casing of 20" was installed from the surface to a depth of 357 m while the production casing of 13 3/8" was installed from the surface to a depth of 919 m. In this case, the fluid was only through the production casing of 13 3/8". Hence, from the above calculation, a cross-sectional area was 0.078 m^2.

3.1. Profile of Well 'X'

3.2.2. Determination of the Coordinates of the Flow Pattern Map

The coordinates (x, y) of the flow pattern map were determined using equations 2 and 3. It was known that on the surface of the well "X" has a dryness (q) of 0.98, a total mass flow (Mtotal) of 23.75 kg/s, a cross-sectional area (Ap) of 0.078 m^2, a water density (ρl) of 893.46 kg/m^3 and a vapor density (ρg) of 4.50 kg/m^3. The determination of the coordinates was conducted through equations 2 and 3 below [18]:

$$x - axis = \frac{Gl^2}{\rho l} = \frac{\left((1-q)\frac{Mtotal}{Ap}\right)^2}{\rho l} \quad (2)$$

$$x - axis = \frac{Gl^2}{\rho l} = \frac{\left((1-0.98)\frac{23.75}{0.078}\right)^2}{893.46}$$

$$x - axis = 2.07\ kg/(ms^2)$$

$$y - axis = \frac{Gg^2}{\rho g} = \frac{\left((1-0.98)\frac{23.75}{0.078}\right)^2}{4.50} \quad (3)$$

$$y - axis = 411.19\ kg/(ms^2)$$

Where:

X-axis, horizontal axis (kg/(ms^2)); *Y-axis*, vertical axis (kg/(ms^2)); Gl, mass flux of liquid phase flowing alone in channel (kg$m^{-2}s^{-1}$) Gg, mass flux of gas phase flowing alone in channel (kg$m^{-2}s^{-1}$); ρl, liquid density (kg/m^3); ρg, gas density (kg/m^3); *q*, dryness; *Mtotal*, total mass (kg/s); *Ap*, the cross-sectional area (m^2)

The results of complete calculations at various depths of the well "X" are displayed in full in Table 1. Then, the results of the x-axis and y-axis are plotted on the Hewitt-Robert flow pattern graph, shown in Figure 3.

Table 1. Calculation result using Hewitt-Robert Method

Depth	Pressure	Enthalpy	Dryness	Casing Size	Ap	Massflow	Water		Steam	
							Density (ρl)	$x - axis$ $\left(\frac{Gl^2}{\rho l}\right)$	Density (ρg)	$y - axis$ $\left(\frac{Gl^2}{\rho g}\right)$
0.00	8.69	2730.77	0.98		0.078	23.75	893.46	2.07	4.50	411.19
50.86	8.72	2730.77	0.98		0.078	23.75	893.29	2.07	4.52	409.71
101.88	8.76	2730.77	0.98		0.078	23.75	893.13	2.07	4.53	408.24
152.91	8.79	2730.77	0.98		0.078	23.75	892.96	2.07	4.55	406.78
203.93	8.82	2730.77	0.98		0.078	23.75	892.80	2.07	4.57	405.33
254.95	8.86	2730.77	0.98		0.078	23.75	892.63	2.07	4.58	403.89
305.98	8.89	2730.77	0.98		0.078	23.75	892.47	2.07	4.60	402.45
357.00	8.92	2730.77	0.98		0.078	23.75	892.30	2.07	4.62	401.03
380.23	8.93	2730.77	0.98	13 3/8"	0.078	23.75	892.24	2.07	4.62	400.48
440.09	8.97	2730.77	0.98		0.078	23.75	892.07	2.07	4.64	399.07
499.95	9.00	2730.77	0.98		0.078	23.75	891.91	2.08	4.65	397.66
559.82	9.03	2730.77	0.98		0.078	23.75	891.74	2.08	4.67	396.27
619.68	9.07	2730.77	0.98		0.078	23.75	891.58	2.08	4.69	394.88
679.54	9.10	2730.77	0.98		0.078	23.75	891.41	2.08	4.70	393.50
739.41	9.13	2730.77	0.98		0.078	23.75	891.25	2.08	4.72	392.14
799.27	9.17	2730.77	0.98		0.078	23.75	891.09	2.08	4.74	390.78
859.14	9.20	2730.77	0.98		0.078	23.75	890.92	2.08	4.75	389.42
919.00	9.23	2730.77	0.98		0.048	23.75	890.76	5.44	4.77	1016.04
947.00	9.25	2730.77	0.98		0.048	23.35	890.69	5.26	4.78	980.61
1000.02	9.28	2730.77	0.98		0.048	23.35	890.55	5.26	4.79	977.80
1063.68	9.31	2730.77	0.98		0.048	23.35	890.39	5.26	4.81	974.44
1127.34	9.34	2730.77	0.98		0.048	23.35	890.23	5.26	4.82	971.11
1191.00	9.38	2730.77	0.98		0.048	22.95	890.07	5.08	4.84	934.92
1243.34	9.41	2730.77	0.98		0.048	22.95	889.93	5.08	4.85	932.30
1307.00	9.44	2730.77	0.98	10 3/4"	0.048	22.45	889.77	4.87	4.87	889.08
1343.00	9.46	2730.77	0.98		0.048	22.25	889.68	4.78	4.88	871.63
1359.00	9.47	2730.77	0.98		0.048	21.75	889.64	4.57	4.88	832.18
1371.00	9.47	2730.77	0.98		0.048	19.15	889.61	3.54	4.89	644.67
1385.00	9.48	2730.77	0.98		0.048	17.15	889.57	2.84	4.89	516.64
1389.00	9.48	2730.77	0.98		0.048	14.15	889.56	1.93	4.89	351.59
1415.00	9.50	2730.77	0.98		0.048	13.15	889.49	1.67	4.90	303.20
1436.70	9.51	2730.77	0.98		0.019	13.15	889.43	10.36	4.90	1879.01
1500.89	9.54	2730.77	0.98		0.019	13.15	889.27	10.36	4.92	1872.54
1567.26	9.58	2730.77	0.98	7"	0.019	13.15	889.10	10.37	4.94	1865.90
1633.63	9.62	2730.77	0.98		0.019	13.15	888.93	10.37	4.96	1859.31
1700.00	9.65	2730.77	0.98		0.019	13.15	888.76	10.37	4.97	1852.76

The Hewitt-Robert flow pattern graph can be used to determine the type of flow pattern using the x-axis and y-axis parameters. Based on the Figure 3, there are 6 types of flow pattern behavior in the geothermal wells, namely bubbly, bubbly slug, churn, annular, and wispy annular. Based on the plotting results of the x-axis and y-axis on the Hewitt-Robert flow pattern graph (Fig. 3), the intersection point of the x-y axis with the line of the annular flow pattern was obtained. Table 2 shows the types of flow patterns based on the results of the plotting shown in the Figure 3.

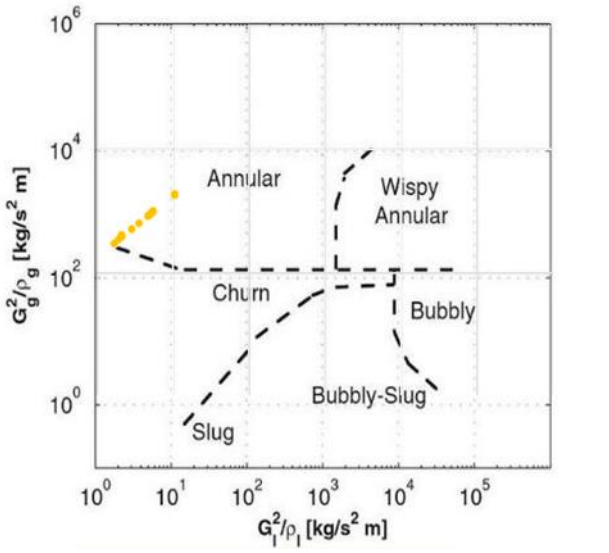

Fig. 3. Plotting the x-axis and y-axis on the Hewitt-Robert Flow Pattern Graph

The results of determining the flow pattern in the well "X" with a range of depths for each casing series as shown in the Figure 3 and Table 2 show that the flow pattern formed was annular. An annular flow is a flow that flows in the internal perimeter of a channel with gas (or vapor) having a higher velocity in the center. This flow pattern is very stable and is the desired flow pattern in piping [19].

Table 2. Flow Patterns based on Hewitt-Robert graph plots

Depth	Water		Steam		Flow Pattern
	Density (ρl)	$x-axis$ $\left(\frac{Gl^2}{\rho l}\right)$	Density (ρg)	$y-axis$ $\left(\frac{Gl^2}{\rho g}\right)$	
0.00	893.46	2.07	4.50	411.19	Annular
50.86	893.29	2.07	4.52	409.71	Annular
101.88	893.13	2.07	4.53	408.24	Annular
152.91	892.96	2.07	4.55	406.78	Annular
203.93	892.80	2.07	4.57	405.33	Annular
254.95	892.63	2.07	4.58	403.89	Annular
305.98	892.47	2.07	4.60	402.45	Annular
357.00	892.30	2.07	4.62	401.03	Annular
380.23	892.24	2.07	4.62	400.48	Annular
440.09	892.07	2.07	4.64	399.07	Annular
499.95	891.91	2.08	4.65	397.66	Annular
559.82	891.74	2.08	4.67	396.27	Annular
619.68	891.58	2.08	4.69	394.88	Annular
679.54	891.41	2.08	4.70	393.50	Annular
739.41	891.25	2.08	4.72	392.14	Annular
799.27	891.09	2.08	4.74	390.78	Annular
859.14	890.92	2.08	4.75	389.42	Annular
919.00	890.76	5.44	4.77	1016.04	Annular
947.00	890.69	5.26	4.78	980.61	Annular
1000.02	890.55	5.26	4.79	977.80	Annular
1063.68	890.39	5.26	4.81	974.44	Annular
1127.34	890.23	5.26	4.82	971.11	Annular
1191.00	890.07	5.08	4.84	934.92	Annular
1243.34	889.93	5.08	4.85	932.30	Annular
1307.00	889.77	4.87	4.87	889.08	Annular
1343.00	889.68	4.78	4.88	871.63	Annular
1359.00	889.64	4.57	4.88	832.18	Annular
1371.00	889.61	3.54	4.89	644.67	Annular
1385.00	889.57	2.84	4.89	516.64	Annular
1389.00	889.56	1.93	4.89	351.59	Annular
1415.00	889.49	1.67	4.90	303.20	Annular
1436.70	889.43	10.36	4.90	1879.01	Annular
1500.89	889.27	10.36	4.92	1872.54	Annular
1567.26	889.10	10.37	4.94	1865.90	Annular
1633.63	888.93	10.37	4.96	1859.31	Annular
1700.00	888.76	10.37	4.97	1852.76	Annular

From the calculation using the WellSim software, there was a mist flow pattern with dryness of 0.98, steam mass 23.26 of kg/s, and brine mass of 0.49 kg/s. A dryness of 0.98 is considered the same along the wellbore because at the time the measurement is only carried out on the surface. The flow pattern obtained should be annular flow because it only produces steam with a dryness of 0.98, which means it is considered a single-phase flow, but because the grouping of flow patterns based on Hewitt-Robert is only for annular flow patterns, the results of calculations and graph plots obtained are annular flow. This annular flow pattern can be thought of as similar to mist flow because it can be found at high vapor quality at the point where the annular flow is thinned by shearing of the gas core at the interface until it becomes unstable so that all the liquid is trapped as droplets in the continuous gas phase [20] .

It can be concluded that based on the manual and software calculations, the well "X" has a vapor fraction of 100% and an annular flow pattern. This annular flow is a flow pattern that is in great demand because it has the highest vapor fraction so it can produce large amounts of steam. In addition, the annular flow is a fairly stable and safe flow, unlike the turbulent flow pattern which can cause large friction and irregular flow [21]. Meanwhile, the flow pattern that is avoided in geothermal wells is a slug flow pattern[22].

3.2.3. Flashing Zone Depth Based on PTS Survey Data

The pressure, temperature, and spinner (PTS) survey is one of the many monitoring activities of geothermal wells, that is routinely carried out on geothermal wells to describe the flow along the wellbore [23].

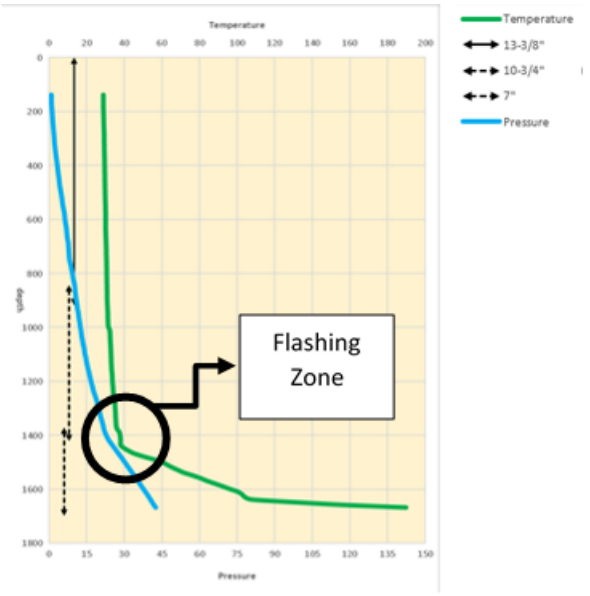

Fig. 4. Graph of PTS injection data

From the flow pattern calculations, at a depth of 1458.27 meters to the surface, there is no brine because the flow pattern formed is annular based on the Hewitt-Robert classification. Based on the PTS injection data in the well "X", it can be seen that this well is a geothermal well that produces steam fluid. This can be seen in Figure 4 showing a constant increase in pressure which means that throughout the production casing from a depth of 1458.27 m to the surface no brine flow can increase pressure. While from a depth of 1458.27 m to 1658.27 m there is a brine flow, this can be seen from the sudden change in pressure and temperature at a certain depth. It can also be seen that the well "X" has a dryness of 0.98 so the well "X" can be called a well with single-phase flow or steam dominated.

The flashing zone is at a depth of about 1458.27 m, because at that depth there is a decrease in pressure from 135 bara to 44 bara due to a change in diameter between the 7" perforated liner which has a small diameter of 6.184" and the 10" perforated liner which has a larger diameter of 9.76". This decrease in pressure will cause steam to come out of the brine which is called flashing.

The flashing will affect the composition of the brine, namely the concentration of scaling is getting thicker due to the loss of some water which turns into steam due to a decrease in pressure and temperature, as well as the release of gases such as CO_2 and H_2S which will affect the pH of the brine. This phenomenon can increase pH and ion concentrations and result in the formation of scaling in the well "X" [24].

$$CaCO_3 + H_2O \leftrightharpoons Ca^{2+} + HCO_3^- + OH^- [19] \quad (4)$$

This phenomenon results in scaling which is the emergence of a problem in the production process of geothermal energy sources in this flash steam system. Therefore, after the flashing area reaches the surface, the steam fluid will flow at a higher speed.

In the analysis of PTS injection data of the well "X", the fluid injection rate at the time of measurement was 75.8 kg/s or 1,200 gpm. Fluid velocity analysis was performed using the slope between the spinner and the cable speed. Figure 5 shows the profile of the slope.

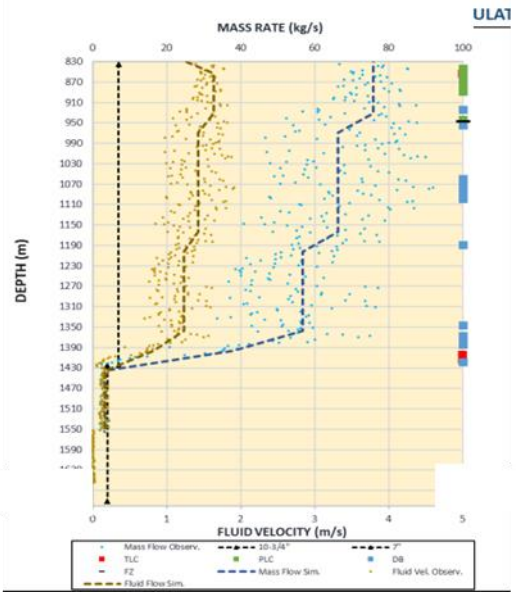

Fig. 5. Graph of Data Velocity, Depth, and Mass Rate

Based on Figure 5, it is known that there are five feedzones, where the feedzone which is in the elevation range of 761-786 m or a depth of 1,389-1,421 m from the ground level has the largest contribution, which is 46%. This shows that the simulation results of mass rate and fluid flow are in accordance with the measurement data. However, the water column that is not formed perfectly causes the results of temperature and pressure measurements to be inconsistent with the measurement data.

3.2.4. Types of Scaling Based on Geochemical Data Analysis

After knowing the accumulation zone of scaling, it is necessary to validate the type of scaling found in the formation and around the liner so that the steam production from the well "X" does not decrease from time to time. From the PTS analysis, there is a flashing zone that can form a scale. This flashing zone results in the formation of steam originating from a decrease in temperature and pressure resulting in the release of H_2S and CO_2 which will affect the pH of the brine.

The geochemical analysis is carried out to determine the fluid content that causes the formation of scaling. Indications of the formation of scaling in the form of silica and calcite can be seen from the value of the saturation index of silica and calcite. If a chemical compound has an index value that exceeds its saturation value (> 1), it means that the scaling is formed in the well[25].

The chemical content of the downhole sample from the well "X" obtained from the geochemical analysis is shown in Table 3.

Table 3. The geochemical analysis results using a downhole sample from the well "X"

Downhole Sampling		
pH Field	8.2	
pH Lab	6.52	
Temp.	254	Celcius
Li	0.029	Ppm
Na	43	Ppm
K	9	Ppm
Ca	52.2	Ppm
Mg	0.36	Ppm
SiO_2	204	Ppm
B	10	Ppm
Cl	6	Ppm
F	5	Ppm
SO_4	170	Ppm
HCO_3	56	Ppm
NH_4	0.1	Ppm
As	0.267	Ppm
Fe	0.165	Ppm

By using the geochemical analysis results (Table 3), the type of scaling in the well "X" can be determined by performing excel calculations on the content of calcite and amorphous silica.

The Calcite Saturation Index (CSI) is calculated using a formula shown in Equation (5) [26].

$$CSI = log \frac{IAP}{Ksp} \quad (5)$$

Where:
CSI, calcite Saturation Index; *IAP*, ion activity product; *Ksp*, solubility product

Before calculating the CSI, it is necessary to know the Ksp of $CaCO_3$. The calculation of Ksp value takes the values of Ca^{2+} and CO_3^{2-} with mole units but the data that has been obtained is still in ppm units (Table 3). If the Ca^{2+} unit is converted from ppm to mol, the Ca^{2+} content of 52.2 ppm will be 0.001305 mol. Because the data obtained is HCO_3 (Table 3), it is necessary to convert its unit from ppm to mol so the HCO_3 of 56 ppm is equal to 0.000918033 mol. Furthermore, the mol of CO_3^{2-} can be calculated using the mol of HCO_3, molecular weight of HCO_3, and molecular weight of CO_3 with the formula shown in equation (6) [25]:

$$CO_3 = \text{Mol } HCO_3 \frac{Mr\ CO_3}{Mr\ HCO_3} \quad (6)$$

$$CO_3 = 0.000918033 \frac{60}{61}$$

$$CO_3 = 0.000902983$$

Where:
Mr, molecule ratio

Furthermore, the Ksp $CaCO_3$ is calculated using the following formula [26]:

$$Ksp(CaCO_3) = [Ca^{2+}] \,.\, [CO_3^{-2}] \quad (7)$$

$$Ksp\ (CaCO_3) = [0.001305] \,.\, [0.000902983]$$

$$Ksp\ (CaCO_3) = 3.3 \times 10^{-9}$$

The solubility product (Ksp) for calcite at a temperature of 25ºC is 3.36×10^{-9} $mol^2.L^{-2}$, where 25ºC is the room temperature because the test was carried out in the laboratory at room temperature. More calcite will form with temperature.

Then, the calculation of the ion activity product (IAP) was conducted with the formula below [26]:

$$Ion = HCO_3 \,.\, Ca \quad (8)$$

$$Ion = 0.000918033 \,.\, 0.001305$$

$$Ion = 1.17839 \times 10^{-6}$$

The ion activity product is the ion of the actual activity of Ca^{2+} and CO_3^{2-} [21]. After getting the Ion and Ksp values, the Calcite Saturation Index (CSI) value can be calculated using the formula (5):

$$CSI = log \frac{IAP}{Ksp} \quad (9)$$

$$CSI = log \frac{1.17839 \times 10^{-6}}{3.3 \times 10^{-9}}$$

$$CSI = 2.54$$

Where:
CSI, calcite Saturation Index; *IAP*, ion activity product; *Ksp*, solubility product

From these calculations, a CSI value of 2.54 was obtained. It can be said that the CSI value was above 1 which indicates that the scaling was formed from calcite in the well "X". The summary of the CSI calculations is shown in Table 4.

Table 4. summary of the CSI calculations

Ca	0.001305
HCO_3	0.000918033
CO_3	0.000902983
Ion	1.17839E-06
Ksp	3.36E-09
CSI	2.544950842

To find out the solubility of amorphous silica formed in brine at vapor pressure, the equation that has been made by Fornier and Truesdell (1973) can be used [26]. The equation is shown in equation (9).

Silica Amorf (SiO_2): t(°C)

$$\left(\frac{731}{(4.52-loglog\ SiO_2)}\right) - 273.15 \quad (10)$$

Before calculating the Silica Saturation Index (SSI), it is necessary to calculate the log SiO_2 first. It is known that the reservoir temperature is 254°C, then it was calculated by the formula [27]:

$$\text{Log } SiO_2 = 4.52 - \left(\frac{751}{(Tres+273)}\right) \quad (11)$$

$$\text{Log } SiO_2 = 4.52 - \left(\frac{751}{(254+273)}\right)$$

$$\text{Log } SiO_2 = 3.094952562$$

Where:
Tres, reservoir temperature (°C)

After the log SiO_2 is known, then the Silica Saturation Index (SSI) calculation is immediately carried out using the formula (10), as follows [28]:

$$\text{SSI} = \left(\frac{731}{(4.52-loglog\ SiO2)}\right) - 273.15 \quad (12)$$

$$\text{SSI} = \left(\frac{731}{(4.52-3.094}\right) - 273.15$$

$$\text{SSI} = 0.850654368$$

From these calculations, the SSI value of 0.85 was obtained. It can be said that the SSI value is still below 1, which means that the silica content is not too saturated or even almost does not form in the X well. At lower temperatures, amorphous silica will be more easily formed than other types of silica. Therefore, amorphous silica is the dominant deposit in surface equipment and wastewater disposal sites [28]. The summary of the SSI calculations is shown in Table 5.

Table 5. summary of the SSI calculations

SiO_2	204
log SiO_2	3.094952562
Silica Amorf	239.8153795
SSI	0.850654368

Based on the CSI and SSI calculations, it can be concluded that the scaling type in the well "X" is scaling from calcite. Based on our experiences, the type of calcite scaling is indeed commonly found in dry stream geothermal wells. The pictures of calcite scaling in the well "X" and the scale stuck in the check valve are shown in Figures 6 and 7, respectively[29].

Fig. 6. Calcite Sample in Well "X"

Fig. 7. Trapped Sample in Check

In previous research by Zolfagharroshan and Khamehchi [30]. only investigate research to predict the scale deposition and modeling production conditions with HOLA software, there has been no detailed explanation regarding the flow pattern that related to scaling in in geothermal wells. However, in this study, we can accumulate zones of scaling and the cause of scaling can be determined by analyzing the flow pattern, characteristics of the fluid, and flashing zones in geothermal wells.

4. Conclusion

Based on the results of this research conducted by the author, it can be concluded that:

a) Based on Hewitt-Robert calculations, the flow pattern formed along the casing series of the well "X" starting from the casing slotted liner 10 " to the surface is an annular type flow pattern.
b) Based on the simulation results using the WellSim software, the flow pattern type in the well "X" is the mist type. This means that there are differences between the results of manual calculation (Hewitt-Robert method) and software calculation (WellSim software). The flow pattern obtained should be a mist flow because it only produces steam, but because the grouping of flow patterns based on Hewitt Robert is only for annular flow patterns, the mist flow is considered the same as annular because it is the closest.
c) According to the flow pattern that has been analyzed, the scaling is possible to be formed in the well "X". Scaling can be formed along the wellbore and in the annular flow zone, which increases with the boiling of the fluid on the casing wall.

d) Based on the analysis using the PTS graph, the zone of accumulation of scaling is at a depth of 1458.27 m located between the casing shoe slotted liners of 7" and 10 3/4".
e) The results of the geochemical analysis show that in the well "X", scaling with calcite and silica types with saturation indexes of 2.54 and 0.85, respectively. It means that the scaling type in the well "X" is calcite scaling.
f) In this research we applied the data as following: geochemical data, PTS data, well's head pressure data, well's production data, flow rate data, well's profile data, and casing summary data and the outcome of the research we can determine flow pattern that can cause scaling and the flashing zone depth. In the future, in order to complete the study, there are some points that need to be research on how to prevent and clean the scaling in the wellbore and also from a financial and development perspective to provide effective and efficient results.

References

[1] I. Ghosh and M. K. Sanyal, "Introspecting predictability of market fear in Indian context during COVID-19 pandemic: An integrated approach of applied predictive modelling and explainable AI," *Int. J. Inf. Manag. Data Insights*, vol. 1, no. 2, p. 100039, Nov. 2021, doi: 10.1016/j.jjimei.2021.100039.

[2] R. Byrtus, R. Hercik, J. Dohnal, J. B. Martinkauppi, T. Rauta, and J. Koziorek, "Low-power Renewable Possibilities for Geothermal IoT Monitoring Systems," *11th IEEE Int. Conf. Renew. Energy Res. Appl. ICRERA 2022*, pp. 164–168, 2022, doi: 10.1109/ICRERA55966.2022.9922835.

[3] P. Angumba, A. Cardenas, and D. Icaza, "Geothermal and Solar Energy Applied to Air Conditioning and Electricity Generation for Homes: Case study Baños in Cuenca-Ecuador," *10th Int. Conf. Smart Grid, icSmartGrid 2022*, pp. 407–413, 2022, doi: 10.1109/icSmartGrid55722.2022.9848548.

[4] S. Z. Ilyas, "Review of the renewable energy status and prospects in Pakistan," *Int. J. Smart grid*, vol. 5, no. 4, 2021, doi: 10.20508/ijsmartgrid.v5i4.220.g174.

[5] A. Harrouz, A. Temmam, and M. Abbes, "Renewable Energy in Algeria and Energy Management Systems," *Int. J. Smart grid*, vol. 2, no. 1, 2017, doi: 10.20508/ijsmartgrid.v2i1.10.g9.

[6] Dewan Energi Nasional Republik Indonesia, "Role of Geothermal in Energy Transition," *www.ruangenergi.com*, 2022. https://den.go.id/index.php/en/dinamispage/index/1332-geothermal-the-sustainable-energy-for-green-recovery-energy-transition-and-security.html (accessed Oct. 12, 2022).

[7] M. E. Shayan, "The Biomass Supply Chain Network Auto-Regressive Moving Average Algorithm," *Int. J. Smart grid*, vol. 5, no. 1, 2021, doi: 10.20508/ijsmartgrid.v5i1.153.g135.

[8] I. G. Association, "Best Practices Guide for Geotherma l Exploration," *IGA Serv. GmbH, Bochum Ger.*, 2014.

[9] N. M. Saptadji, *Teknik panasbumi*. Bandung: ITB University Press, 2001.

[10] E. Gunnlaugsson, H. Ármannsson, S. Thorhallsson, and B. Steingrímsson, "Problems in geothermal operation-scaling and corrosion," Santa Tecla, 2014.

[11] C. Sapto and P. Salvius, *Evaluasi Potensi Silica Scaling Pada Pipa Produksi Lapangan Panasbumi Lahendong – Sulawesi Utara*. Yogyakarta: Yogyakarta, 2001.

[12] E. T. S. Agustinus, I. Syafri, M. F. Rosana, and I. Zulkarnain, "Scale Prevention Technique to Minimized Scaling on Re-Injection Pipes in Dieng Geothermal Field, Central Java Province, Indonesia," *Indones. J. Geosci.*, vol. 5, no. 2, 2018, doi: 10.17014/ijog.5.2.129-136.

[13] E. Widodo, A. Akbar, and J. Timur, "Pengaruh Konsentrasi Garam Terhadap Karakterisitik Aliran Dua Fase Gas Dan Air," Universitas Muhammadiyah Sidoarjo, 2015.

[14] M. Flores Armenta, M. Ramírez Montes, and L. Morales Alcala Alejandro Volta, "Wellbore Modeling of Production Well H-1D using WellSim, Los Humeros Geothermal Field, México," *Proc. World Geotherm. Congr.*, no. April, pp. 19–25, 2015.

[15] E. Tolivia, "Flow in geothermal wells (An analytical study)," *Geothermics*, vol. 1, no. 4, pp. 141–145, 1972, doi: 10.1016/0375-6505(72)90023-5.

[16] R. Idroes and M. Yusuf, "Geochemistry exploration and geothermometry application in the North Zone of Seulawah Agam, Aceh Besar District, Indonesia," *Energies*, vol. 12, no. 23, 2019, doi: 10.3390/en12234442.

[17] P. S. Hsieh, C. K. Lin, Y. Te Chang, H. Y. Lu, and T. F. Yang, "The GTFSampler: A new downhole equipment for geothermal fluid sampling and its testing results in the Chingshiu geothermal field, Ilan, Taiwan," *Geothermics*, vol. 94, no. 195, p. 102077, 2021, doi: 10.1016/j.geothermics.2021.102077.

[18] K. Nicholson, *Geothermal Fluids*. 1993. doi: 10.1007/978-3-642-77844-5.

[19] J. R. Thome, "Engineering Data Book III : Enhanced heat transfer design methods for tubular heat exchangers," 2016.

[20] J. R. Thome and A. Cioncolini, *Two-Phase Flow Pattern Maps for Microchannels*, no. October. 2015. doi: 10.1142/9789814623216_0020.

[21] T. Ganat and M. Hrairi, "Effect of flow patterns on two-phase flow rate in vertical pipes," *J. Adv. Res. Fluid Mech. Therm. Sci.*, vol. 55, no. 2, pp. 150–160, 2019.

[22] A. Rahmandhika, A. Saifullah, P. R. Ansyah, and A. Mokhtar, "Effect of Liquid Hold-Up on Transition of 2-Phase Air-Air Flow Pattern from Stratified To Slug in 50 mm Pipe," *J. Sci. Appl. Technol.*, vol. 4, no. 2, p. 75, 2020, doi: 10.35472/jsat.v4i2.279.

[23] Herianto, "Analisis Data Pressure Temperature Spinner Untuk Penentuan Potensi Sumur Panas Bumi 'RB-1' Lapangan Kerinci," pp. 9–25, 2019.

[24] Solenis, "Cutting-Edge Scale Control Solutions For Geothermal Power Producers (EMEA And APAC)," *Solenis.com*, 2021. https://www.solenis.com/en/resources/events/webinars/cutting-edge-scale-control-solutions-for-geothermal-power-producers-emea-apac (accessed Sep. 18, 2021).

[25] M. B. Furqan, "Evaluation of the Success of Matrix Acidizing and Well Washing Geothermal Wells Mbf –

246 and Miz – 153 Field F - 25," *Semin. Nas. Cendekiawan 2015*, pp. 571–581, 2015.

[26] B. Köhl, M. Elsner, and T. Baumann, "Hydrochemical and operational parameters driving carbonate scale kinetics at geothermal facilities in the Bavarian Molasse Basin," *Geotherm. Energy*, vol. 8, no. 1, 2020, doi: 10.1186/s40517-020-00180-x.

[27] R. O. Fournier and A. H. Truesdell, "An empirical NaKCa geothermometer for natural waters," *Geochim. Cosmochim. Acta*, vol. 37, no. 5, pp. 1255–1275, 1973, doi: 10.1016/0016-7037(73)90060-4.

[28] M. Tassew, "Effect of solid deposition on geothermal utilization and methods of control," no. 13, pp. 1–20, 2001.

[29] PT. Geodipa Energi Unit Patuha, "Report of Well Logging And Investigation Patuha Unit 1 Year 2020," Bandung, 2021.

[30] M. Zolfagharroshan and E. Khamehchi, "A rigorous approach to scale formation and deposition modelling in geothermal wellbores," *Geothermics*, vol. 87, no. March, p. 101841, 2020, doi: 10.1016/j.geothermics.2020.101841.